

Journal Pre-proofs

Selective laser sintering additive manufacturing of dosage forms: Effect of powder formulation and process parameters on the physical properties of printed tablets

Evgenii Tikhomirov, Michelle Ahlén, Nicole Di Gallo, Maria Strømme, Thomas Kipping, Julian Quodbach, Jonas Lindh

PII: S0378-5173(23)00200-4
DOI: <https://doi.org/10.1016/j.ijpharm.2023.122780>
Reference: IJP 122780



To appear in: *International Journal of Pharmaceutics*

Received Date: 5 December 2022
Revised Date: 20 February 2023
Accepted Date: 22 February 2023

Please cite this article as: E. Tikhomirov, M. Ahlén, N. Di Gallo, M. Strømme, T. Kipping, J. Quodbach, J. Lindh, Selective laser sintering additive manufacturing of dosage forms: Effect of powder formulation and process parameters on the physical properties of printed tablets, *International Journal of Pharmaceutics* (2023), doi: <https://doi.org/10.1016/j.ijpharm.2023.122780>

This is a PDF file of an article that has undergone enhancements after acceptance, such as the addition of a cover page and metadata, and formatting for readability, but it is not yet the definitive version of record. This version will undergo additional copyediting, typesetting and review before it is published in its final form, but we are providing this version to give early visibility of the article. Please note that, during the production process, errors may be discovered which could affect the content, and all legal disclaimers that apply to the journal pertain.

1 **Selective laser sintering additive manufacturing of dosage forms: Effect of powder**
2 **formulation and process parameters on the physical properties of printed tablets**

3 Tikhomirov, Evgenii¹, Åhlén, Michelle¹, Di Gallo, Nicole², Strømme, Maria¹, Kipping,
4 Thomas², Quodbach, Julian^{3,*}, Lindh, Jonas^{1,*}

5 ¹Division of Nanotechnology and Functional Materials, Department of Materials Science
6 and Engineering, Ångström Laboratory, Uppsala University, Uppsala SE-751 03, Box 35,
7 Sweden.

8 ²Merck KGaA, Frankfurter Str. 250, Postcode: D033/001, Darmstadt DE-642 93,
9 Germany.

10 ³Department of Pharmaceutics, Utrecht Institute for Pharmaceutical Sciences, Utrecht
11 University, Universiteitsweg 99, 3584 CG Utrecht, The Netherlands

12 **Corresponding authors:** Jonas Lindh Jonas.Lindh@angstrom.uu.se, Julian Quodbach
13 j.h.j.quodbach@uu.nl

14 **Keywords:** Additive manufacturing, Three-dimensional printing, Selective laser
15 sintering, Personalized medicines, Drug manufacturing

16 **Abstract**

17 Large batches of placebo and drug-loaded solid dosage forms were successfully
18 fabricated using selective laser sintering (SLS) 3D printing in this study. The tablet
19 batches were prepared using either copovidone (N-vinyl-2-pyrrolidone and vinyl acetate,
20 PVP/VA) or polyvinyl alcohol (PVA) and activated carbon (AC) as radiation absorbent,
21 which was added to improve the sintering of the polymer. The physical properties of the
22 dosage forms were evaluated at different pigment concentrations (i.e., 0.5 and 1.0 wt%)
23 and at different laser energy inputs. The mass, hardness, and friability of the tablets were

24 found to be tunable and structures with greater mass and mechanical strength were
25 obtained with increasing carbon concentration and energy input. Amorphization of the
26 active pharmaceutical ingredient in the drug-loaded batches, containing 10 wt% naproxen
27 and 1 wt% AC, was achieved *in-situ* during printing. Thus, amorphous solid dispersions
28 were prepared in a single-step process and produced tablets with mass losses below 1
29 wt%. These findings show how the properties of dosage forms can be tuned by careful
30 selection of the process parameters and the powder formulation. SLS 3D printing can
31 therefore be considered to be an interesting and promising technique for the fabrication
32 of personalized medicines.

33 **1. Introduction**

34 Conventional drug formulations for oral administration are limited to only a few available
35 dosage forms. Manipulations of such dosage forms are often carried out when treating
36 particular patient groups with diverse and specific needs, e.g., pediatric patients [1, 2].
37 According to two independent studies carried out in Sweden and the Netherlands, drug
38 manipulations occurred in 15% [1] to 60% [2] of cases in hospitals, depending on the age
39 group and diagnoses of the patients. The most vulnerable patients were found to be
40 toddlers and pre-school children, who require small dosage forms, which were typically
41 prepared from commercially available pharmaceutical preparations as a slurry. However,
42 only 41% of these medicines were prepared and manipulated according to the Summary
43 of Product Characteristics (SmPc) or Package Information Leaflet (PIL) requirements [2].
44 This may lead to inaccurate dosing and such incorrect treatment could pose a serious risk
45 in the remaining 59% of cases when these requirements were not followed. This
46 demonstrates that the administration of oral medicines remains an issue not only for
47 pediatrics but also for the treatment of other heterogeneous patient groups such as

48 geriatric patients [3-5]. Where the uses of off-label medications often lead to inefficient
49 treatment due to differences between the pharmacogenetic and pharmacokinetic
50 characteristics of these individuals and the general adult population [4, 6]. 3-dimensional
51 printing (3D printing), however, has emerged during the last decade as a promising
52 technique for the fabrication of personalized dosage forms. Structures of great complexity
53 and intricacy, prepared using computer-aided design (CAD) software, have been obtained
54 from various layer-by-layer deposition methods with relative ease [4]. As such, the
55 technique could prove useful for manufacturing dosage forms with bespoke properties
56 (i.e., geometries, drug release profiles, and appearances) on-demand and locally at
57 hospitals according to each patient's needs [7]. Various 3D printing technologies have
58 been investigated for the printing of medicines, including fused-deposition modeling
59 (FDM) [8-10], binder jetting [11, 12], stereolithography (SLA) [13-15], and selective
60 laser sintering (SLS) [16-19], to name a few. In particular, the SLS technique may offer
61 certain advantages, as compared to other 3D printing techniques, for the manufacturing
62 of larger batches of dosage forms (e.g., 30 or 100 tablets per print) due to the instrument's
63 large print volume and high packing density. The technique utilizes a laser beam at a
64 certain wavelength as a source of energy to selectively fuse powder particles on the
65 surface of a powder bed. Depending on the desired power and optical properties of the
66 initial powder formulation the laser type may vary from laser diodes to CO₂-lasers [20].
67 The 3D structures are further constructed through the fusion and attachment of the
68 sintered layers to each other and are stabilized in the build volume by the surrounding un-
69 sintered powder. The SLS technique, therefore, does not require the use of additional
70 supports which are typically required in FDM or SLA printing. Absorbing pigments, in
71 the form of e.g. active carbons or iron oxide, are usually needed to enhance the sintering

72 of the powders if the wavelength of the laser is in the IR- or Vis-region [5, 19, 21-23].
73 The formation of amorphous solid dispersions (ASDs) from various active
74 pharmaceutical ingredients (APIs) and polymers has also been demonstrated through SLS
75 printing [24-27]. Thus, this shows that the technique may be promising for the
76 manufacturing of dosage forms containing biopharmaceutical (BCS) class II or IV poorly
77 water-soluble drugs [28-30].

78 In this study, we present the fabrication of batches of 30 tablets of PVP/VA and
79 PVA-based placebo and naproxen-loaded tablets using selective laser sintering 3D
80 printing. The physical properties of the printed tablets, as a function of pigment
81 concentration and laser energy input, were evaluated using powder X-ray diffraction and
82 differential scanning calorimetry. A thorough analysis of the dimensions, weights, and
83 friability of the tablets was carried out. The correlation between tablet hardness and
84 printing-angle was further studied in order to investigate the anisotropy of the printed
85 structures.

86 **2. Materials and methods**

87 *2.1. Materials*

88 Activated carbon (powder, mesh size 100, which corresponds to particles that passed
89 through a sieve of 149 μm) was purchased from Sigma-Aldrich, USA. PVP/VA (Plasdone
90 S-630, 60:40 linear copolymer of N-vinyl-2-pyrrolidone and vinyl acetate) was kindly
91 provided by Ashland Industries Deutschland GmbH (Düsseldorf, Germany), and PVA
92 (Parteck® MXP, polyvinyl alcohol, PVA), Aerosil (highly dispersed colloidal silica,
93 SiO_2), and Naproxen manufactured by Fagron (Rotterdam, Netherlands) were generously
94 provided by the Merck Group (Darmstadt, Germany).

95 All chemicals were used as received without further processing.

96 *2.2. Powder preparation*

97 Placebo and naproxen-loaded powder formulations were prepared according to Table 1.
 98 The compound names consist of three or five letters in the beginning which corresponds
 99 to selected polymer (i.e., PVP/VA or PVA) and the presence of the API (N – Naproxen).
 100 The second part of the name is the digit (0.5 or 1) which defined the AC weight
 101 percentage. All powder mixtures were sieved using a 315 μm stainless-steel test sieve
 102 (VWR International AB, Sweden) and mixed using a Turbula shaker (Turbula T2F
 103 shaker, Glen Mills, Inc., Clifton, NJ, US) for 15 min. AC and fumed silica were added to
 104 the formulations in order to enhance the laser energy absorption of the powders and to
 105 improve powder flowability during the printing process, respectively. The formulations
 106 were prepared in large enough batches (> 1000 mL) to partially fill the build volume (150
 107 x 200 x 150 mm).

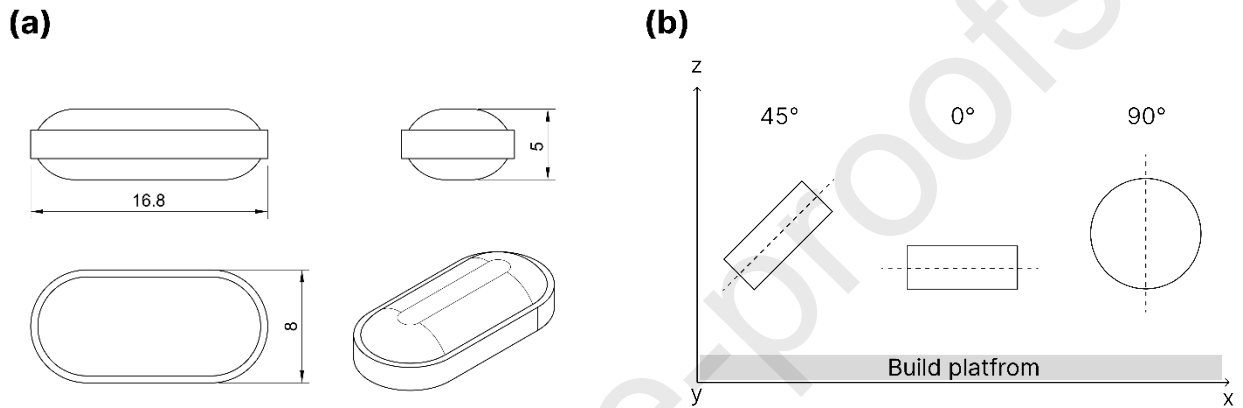
108 **Table 1.** Composition of the prepared powder formulations used in this study.

Compound	PVA-05 (wt%)	PVA-1 (wt%)	PVA-N-1 (wt%)	PVP/VA-05 (wt%)	PVP/VA-1 (wt%)	PVP/VA-N-1 (wt%)
PVA	99	98.5	88	-	-	-
PVP/VA	-	-	-	98.5	98	88
AC	0.5	1	1	0.5	1	1
Aerosil (fumed silica)	0.5	0.5	1	1	1	1
Naproxen	-	-	10	-	-	10

109 *2.3 Selective laser sintering 3D printing of dosage forms*

110 Tablet models (Figure 1) were created and designed in Solidworks 2019 SP05 (Dassault
 111 Systèmes Corporation, Vélizy-Villacoublay, France), and the obtained stereolithography

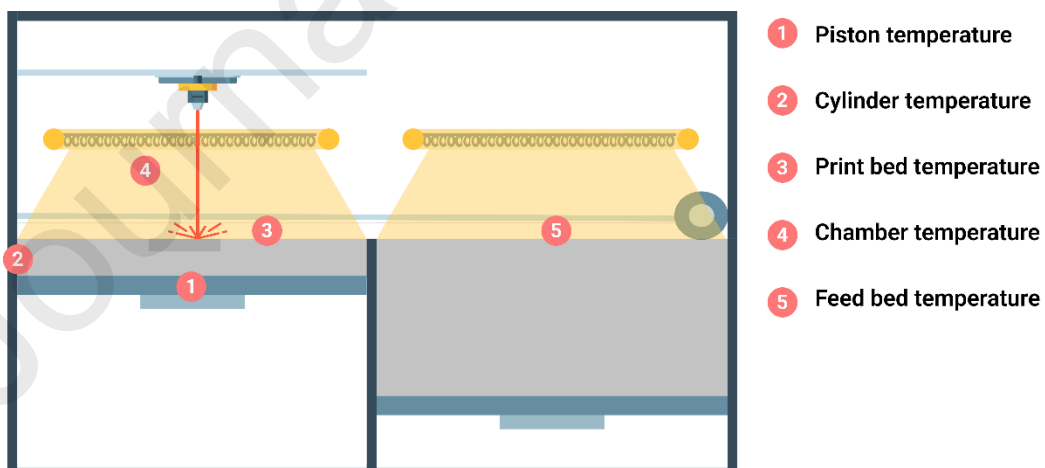
112 file (STL) was subsequently prepared for printing in Sinterit Studio 2019 1.7.0.1 (Sinterit
 113 sp. z o.o., Krakow, Poland) using the process parameters presented in Table S1 – S2. The
 114 software allows for set up and adjustment of various parameters including temperatures,
 115 model location, and position inside of the chamber (Figure 1b), layer height as well as
 116 laser power ratio (LPR).



117

118 **Figure 1.** (a) Orthographic projection and a 3D model of the dosage form, all units are
 119 given in mm, and (b) cylindrical tablets orientation scheme with respect to the
 120 build platform.

121 There are five parts of which the temperatures can be controlled inside of the printer
 122 which are shown in Figure 2.



123

124 **Figure 2.** Schematic drawing of the Sinterit Lisa SLS 3D Printer showing the various
 125 temperature elements which may be varied for each printing process.

126 The 3D printing process was further carried out as follows: the prepared powder
127 formulations (Table 1) were placed in the powder reservoir (150 x 200 x 150 mm) of the
128 SLS 3D printer (Sinterit Lisa SLS 3D printer, Sinterit, Kraków, Poland). A thin layer of
129 the formulation was thereafter spread onto the build platform after which the powder beds
130 were slowly heated to the temperatures specified in Table S1 – S2. The sintering process
131 was carried out using a 5 W infrared laser diode ($\lambda = 808$ nm) in accordance with the
132 template models given in the STL-file in a layer-by-layer fashion. A total of 30 tablets
133 were printed per batch, at a 45° angle to the build platform (i.e. orthogonal to the x - y
134 plane, see Figure 1b), using a layer height of 150 μ m. Cylindrical tablets (h = 4 mm, d =
135 10 mm) were additionally printed at three different angles to the build platform, namely
136 0°, 45°, and 90° (with respect to the x - y -plane, Figure 1b), in order to evaluate the
137 mechanical properties of the tablets. Specific values for the laser energy transmitted upon
138 the active layer were chosen when printing the different batches. So-called laser power
139 ratio (LPR) is used as a laser power adjustment variable which is defined as a
140 multiplication coefficient of the initial energy output (5 W) and does not have a certain
141 unit. In this study the LPR values 2, 2.5, and 3 were used. The finished batches were
142 retrieved from the build platform at the end of the printing process by sieving. The tablets
143 were additionally de-dusted using pressurized air in order to remove excess powder and
144 stored in sealed containers for further analysis.

145 2.4 Characterization

146 Powder X-ray diffraction (PXRD) diffractograms of pristine and heat-treated powder
147 formulations as well as the printed dosage forms were collected on a Bruker D8 Advance
148 TwinTwin diffractometer (Bremen, Germany) using Cu-K α ($\lambda = 1.5418$ Å) radiation. The
149 instrument was operated at 40 mA and 40 kV, using a step-size of 0.02°, and a data

150 collection time of 1 h. Differential scanning calorimetry (DSC) thermograms were
151 obtained on a Mettler Toledo DSC 3+ (Schwerzenbach, Switzerland) using a heating and
152 cooling rate of 10 °C min⁻¹ and nitrogen as purge-gas. Repeated heating-cooling
153 measurements were carried out from -40 to 200 °C and from 200 to 10 °C in the first
154 cycle, and from 10 to 200 °C in the following cycles (presented in Figures S3 and S4).
155 X-ray micro-computed tomography (μCT) was performed on a CT-Alpha (Procon X-
156 Ray, Sarstedt, Germany) with following reconstruction in VG Studio (Volume Graphics
157 D, Germany). The instrument was operated at 80 kV and 30 mA, using a voxelsize of 10
158 μm and exposure time of 500 ms. A total of 1600 projections were collected for each
159 measured sample and used for the porosity analysis. The porosity of the printed structures
160 was calculated as the ratio between the volume fraction of the pores and the total volume
161 of the printed structure. The Avizo 3D 2022.2 software (Thermo Fisher Scientific Inc.,
162 USA) was used for the analysis. The dimensions (n = 10) and weights (n = 30) of the
163 printed tablet were examined using a digital caliper and an analytical balance (Mettler
164 Toledo XS 64 Analytical Balance, Schwerzenbach, Switzerland). Friability tests were
165 carried out in accordance with the European Pharmacopoeia 2.9.7 [31] on approx. 6.5 g
166 of tablets using a Pharmatest PTF E Friabilator (Hainberg, Germany) at 25 rpm and for
167 100 rotations. The tablets were carefully weighed pre- and post-measurement and the total
168 weight loss of the tablets (i.e., friability) was calculated. Measurements of the breaking
169 force (given in Newtons, N) were obtained from diametrical compression tests carried out
170 on ten cylindrical tablets (10 mm in diameter) from batches printed at different angles to
171 the printing platform. The Pharmatest PTB 311E tablet hardness testing instrument
172 (Hainberg, Germany) was used in the current study.

173 *2.5 In-vitro dissolution tests of printed tablets*

174 Dissolution tests were carried out using a Sotax AT7 Smart Dissolution Tester (Aesch,
175 Switzerland) according to USP guidelines [32]. *In-vitro* drug release profiles for the 3D
176 printed tablets (n = 3) were recorded at pH 7.4 (phosphate buffer, 900 mL) at 37 ± 0.5 °C
177 and 50 rpm using a sinker to weigh down the tablets. The drug concentration in the
178 dissolution media was determined with high performance liquid chromatography (HPLC)
179 (Agilent 1260 Infinity II, Agilent Technologies, Inc., Santa Clara, USA) on 20 μ L of pre-
180 filtered media (0.45 μ m PTFE filters, VWR International GmbH). The HPLC assays were
181 performed at 25 °C using a mobile phase composition of acetonitrile–Milli-Q water–
182 acetic acid (49.45:9.45:1.10 v.v%). Samples were injected into a Kinetex 5u C8 100A
183 column (150 x 4.6 mm, Phenomenex, Inc. Torrance, CA, USA) at a flow-rate of 1.2 mL
184 min^{-1} and the eluent analyzed spectroscopically at 254 nm.

185 *2.6 Determination of tablet drug loading*

186 The drug content uniformity of the 3D printed tablets (n = 5) were evaluated by placing
187 the individually pre-weighed tablets into 100 ml volumetric flasks containing 50 ml Milli-
188 Q water. The tablets were stirred at 37 °C and 500 rpm for 1 h, after which the solutions
189 were diluted with HPLC mobile phase, filtered (0.45 μ m PTFE filters, VWR International
190 GmbH) and analyzed using the same HPLC method as specified in *section 2.5*.

191 *2.7 Statistical analysis*

192 Statistical analysis of the weight distributions of the printed tablets were calculated using
193 one-way ANOVA and weight probability density distributions were constructed in
194 RStudio 1.4.1717 (RStudio PBC, Boston, USA).

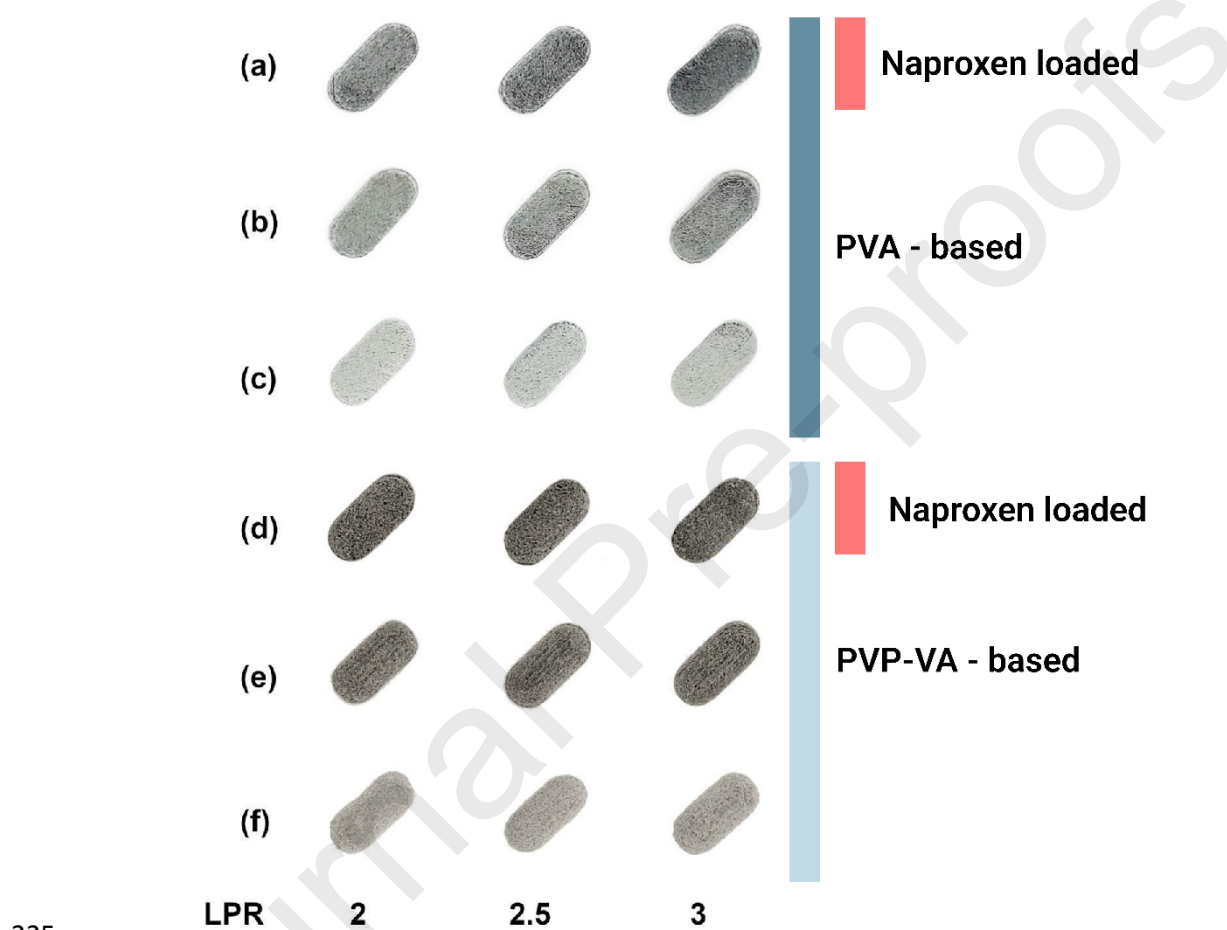
195 **3. Results and discussion**

196 *3.1. Solid state characterization of SLS-printed tablets*

197 The printed dosage forms (Table 1 and Tables S1 – S2) were prepared from either placebo
198 formulations containing 0.5 – 1 wt% AC as colorant or from drug-loaded powder
199 mixtures with 10 wt% naproxen as active pharmaceutical ingredient (API), and 1 wt%
200 AC. Previous studies have shown carbon to be a suitable pigment for the fabrication of
201 paracetamol-based printlets [33] as well as metronidazole-loaded carbon-reinforced
202 polyamide 12 (PA 12) composite printlets [34]. Other excipients may also be used as
203 absorbing material in order to provide sufficient thermal energy to sinter various polymers
204 in the presence of NIR/IR lasers. One such example includes the combination of the
205 Kollicoat® IR and an IR-absorbing dye [35]. Well-sintered tablets with no observable
206 defects were obtained from all prepared powder formulations at LPRs between 2 to 3. As
207 can be seen in Figure 3, a clear and expected difference in shading could be observed
208 between the different batches containing 0.5 – 1 wt% AC and naproxen. The appearance
209 of the tablets was found to be influenced to a lesser degree by the LPR, especially for
210 batches containing 0.5 wt% carbon. However, minor differences in shading between
211 different LPRs were still observable. Which shows the effects that an increased energy
212 input of the laser may have on the visual appearance of the printed tablets (i.e., darkening
213 of the tablet due to a higher degree of sintering).

214 The laser properties may be described differently, depending on the printer and the laser
215 system inside. For instance, another frequently used SLS printer, Sintratec Kit, uses a
216 galvo-system, which is defined by the scanning speed. In case of the Sinterit printer used
217 in the current study, the more cryptic term LPR defines the laser energy input. Even
218 though the laser systems are different, the output is the same - an energy density that
219 represents the amount of the energy initially emitted upon the active powder layer. The
220 energy density of the laser beam not only affects the appearance of tablets but the

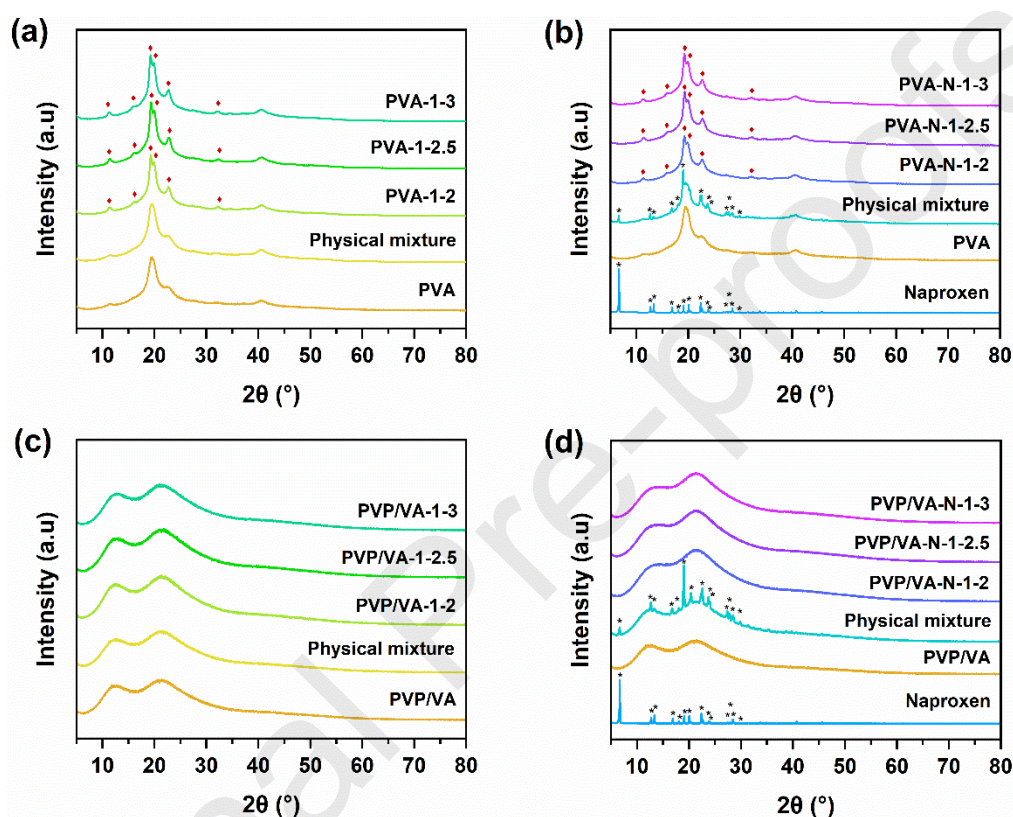
221 mechanical and dissolution properties, which has been observed in other studies [26, 36,
 222 37]. The selection of suitable printing parameters such as LPR or scanning speed and
 223 temperatures depends on the thermal and physical properties of the specific polymers,
 224 APIs, and colorants [26, 28, 38].



226 **Figure 3.** The camera images of PVA- (a – c) and PVP/VA (d – f) tablets containing (a
 227 and d) 10 wt% naproxen and 1 wt% AC, (b and e) 1 wt% AC, and (c and f) 0.5 wt%
 228 AC. Images were taken at the same light conditions and camera settings.

229 The crystalline state of the API and polymers in the printed dosage forms was evaluated
 230 by PXRD and DSC. Diffractograms of the printed batches containing 1 wt% AC, their
 231 corresponding physical mixtures, and the pristine polymer and API are shown in Figure 4.
 232 The diffractograms of the placebo dosage forms can be seen to correspond to that of the
 233 pristine polymers with some additional emerging peaks for the PVA-based tablets

234 characteristic to that of crystalline PVA at approximately $2\theta = 11.34^\circ, 16.01^\circ, 19.33^\circ,$
 235 $19.98^\circ, 22.77^\circ, 27.46^\circ,$ and 32.33° [39]. No peaks corresponding to the API were observed
 236 for either batch of naproxen-loaded tablets, indicating that a majority of the drug in the
 237 powder formulations was successfully amorphized during the printing process.



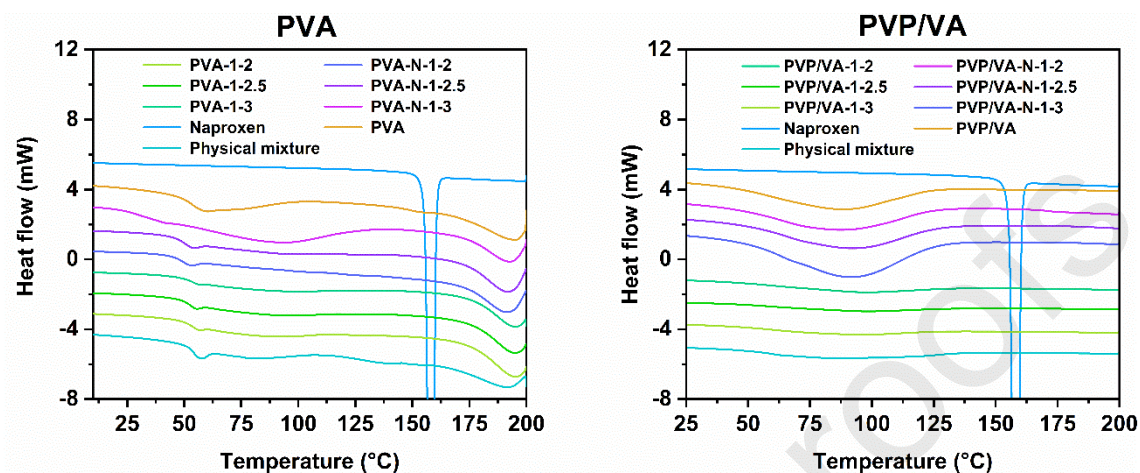
238

239 **Figure 4.** PXRD diffractograms ($\lambda = 1.5418 \text{ \AA}$) of printed placebo and naproxen-loaded
 240 solid dosage forms. Phases corresponding to crystalline polyvinyl alcohol and naproxen
 241 are highlighted with red diamond symbols and black asterisks, respectively.

242 DSC thermograms of the printed tablets (Figure 5) were found to be in good agreement
 243 with observations made from the diffractograms. A single glass transition (T_g) event
 244 along with an overlapping enthalpy of relaxation peak could be observed for all the PVA-
 245 based dosage forms as well as the pristine polymer. Indicating that the API in the
 246 naproxen-loaded tablets was molecularly dispersed in the polymer and that an amorphous
 247 solid dispersion (ASD) had successfully been obtained [40]. A shift in T_g of
 248 approximately 1.5 and 3.5 $^\circ\text{C}$, as compared to the pristine polymer, was seen for the

249 placebo and naproxen-loaded batches, respectively, further indicating that the colorant
250 and/or API may act as weak plasticizers. The thermograms of the PVP/VA-based dosage
251 forms, on the other hand, showed no discernable glass transition in the measured
252 temperature interval. This was found to be due to the broad endothermic peak at
253 approximately 90 °C corresponding to the desorption of water in the polymer in the first
254 heating cycle, which coincides with the reported T_g of PVP/VA (i.e. Plasdone S-630) at
255 109 °C [41]. No melting peak corresponding to naproxen at 158.5 °C was observed for
256 either drug-loaded batch, confirming the amorphous state of the API in the printed tablets.
257 Notably, such events were also found to be absent in the physical mixtures. The
258 combination of DSC and PXRD is widely used to identify traces of crystalline material
259 [40] and is suitable for different types of drugs with different melting peaks, such as
260 Paracetamol ($T_m = 172$ °C) [42] or Naproxen ($T_m = 158.5$ °C), in the current study. In both
261 cases, the melting endotherm in the DSC profile disappears after the sintering process,
262 which is caused by the dissolution of the API into the polymer matrix at the temperature
263 above T_g of the polymer regardless of the melting temperature of the API. This
264 demonstrates that the API was able to dissolve in the polymer matrices below the melting
265 point of the drug, thus showing that ASDs may be formed using either PVA or PVP/VA.
266 In the case of PVP/VA, the dissolution of the API in the polymer likely occurred between

267 109 to 158 °C at the flowing point, T_f , of the polymer (i.e. the temperature at which the
 268 polymeric chains gain greater mobility and the polymer enters a viscous liquid state) [38].



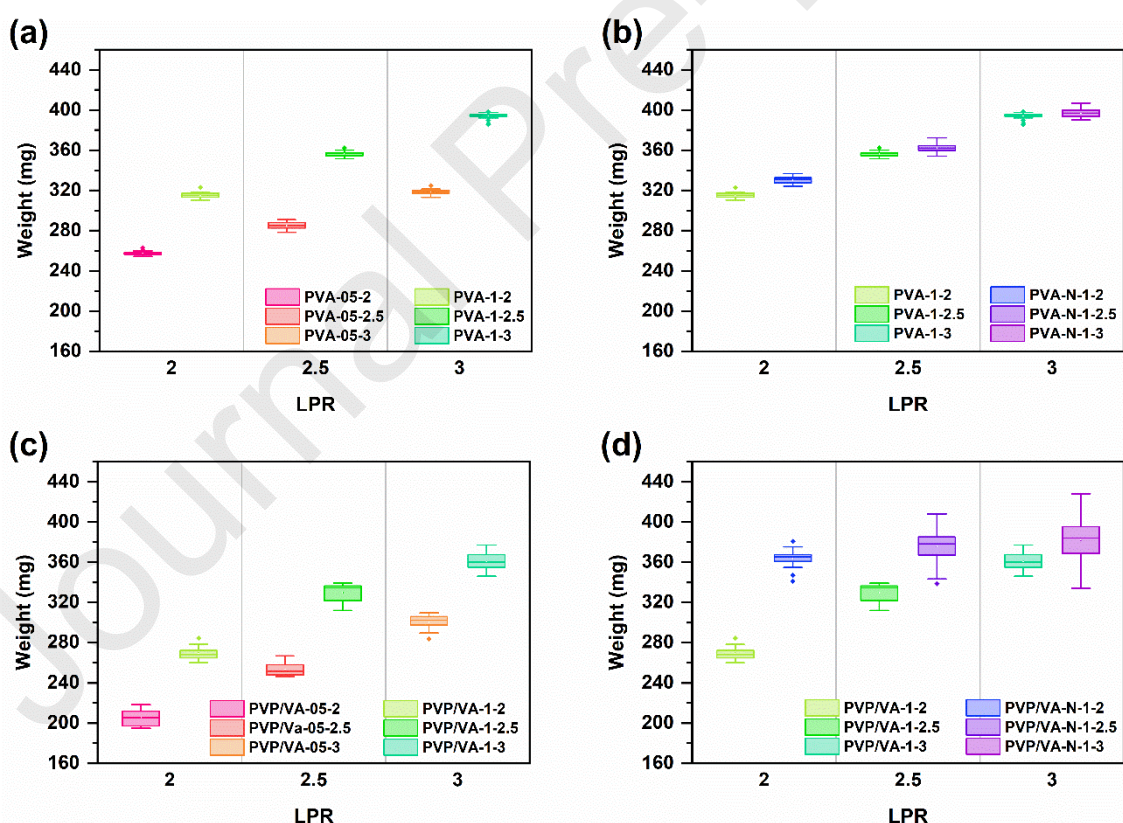
269

270 **Figure 5.** DSC thermograms of naproxen-loaded and placebo tablets containing 1 wt%
 271 AC along with the pristine polymers and API. Presented thermograms represent the first
 272 heating cycle.

273 3.2 Weight uniformity and tablet dimensions

274 The recorded mass of the placebo tablets containing 0.5 and 1 wt% AC as well as the
 275 naproxen-loaded tablets are presented in Figure 6, Figure S6, and Tables S4 – S5. A
 276 significant difference ($P < 0.05$) between the weight distributions of the placebo tablets
 277 could be seen. Indicating that the average tablet weight could be effectively controlled by
 278 the addition of more colorant. An overlap in the mass distributions could be seen for PVA-
 279 05-3 and PVA-1-2 (Figure 6a) as well as PVP/VA-05-3 and PVP/VA-1-2 (Figure 6c),
 280 i.e., batches printed with the highest and lowest LPR using 0.5 wt% and 1 wt% AC,
 281 respectively. Demonstrating that tablets of comparable weight may be obtained at
 282 different colorant concentrations by varying the LPR. Comparisons between the
 283 naproxen-loaded batches (PVA-N-1) and placebo tablets (PVA-1) containing 1 wt% AC
 284 also show that the obtained PVA-based tablets were similar in mass. An increase in
 285 average tablet weight by 4.79, 1.66, and 0.63 wt% was observed for the naproxen-loaded
 286 batches as compared to the placebo tablets when the LPR was increased. According to

287 the acquired data, the weight and weight distributions depend on the polymer selection
 288 even though other concentrations and printing parameters were kept the same. The main
 289 reason for this behavior is the thermal properties of polymers, especially T_g . Previous
 290 studies have shown a strong correlation between poor printability (insufficient sintering
 291 resulting in extremely low tablet weights) and the high value of T_g [21, 43, 44]. Similar
 292 trends were however not detected for the PVP/VA-based dosage forms, where significant
 293 weight differences between the naproxen-loaded tablets were observed for all batches
 294 aside from PVP/VA-N-1-2.5 and PVP/VA-N-1-3. Indicating that smaller increments in
 295 LPR and carbon concentration may be required in order to tune the tablet weight in such
 296 formulations.



297

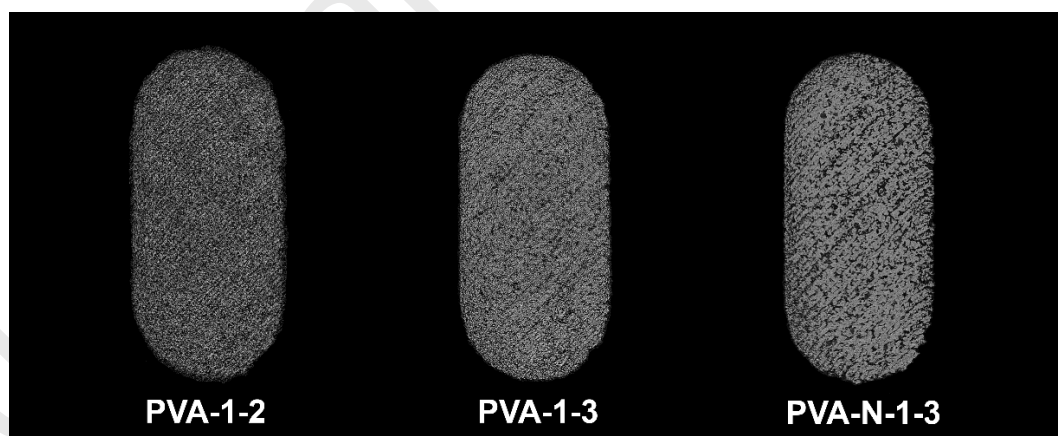
298 **Figure 6.** Box-plots showing the weight distributions of (a) PVA-based placebo tablets
 299 containing 0.5 and 1 wt% AC, (b) naproxen-loaded PVA-based tablets containing 1 wt%
 300 AC, (c) PVP/VA-based placebo tablets containing 0.5 and 1 wt% AC, and (d) naproxen-
 301 loaded PVP/VA-based tablets containing 1 wt% AC.

302 The dimensions of the printed tablets were found to remain consistent across all batches,
303 only increasing slightly with colorant concentration, drug loading, or LPR, especially for
304 the PVP/VA-based tablets (Tables S4 and S5). This indicates that the observed increase
305 in tablet weight was related to a densification of the printed structures and not to an
306 increase of their dimensions. However, it is important to note that small deviations in the
307 tablet volume, which may be too small to accurately measure using a caliper, could
308 contribute significantly. An average deviation of 2.31, 1.53, 0.42 wt% and 3.49, 7.22,
309 2.19 wt% in the length, height, and width of the PVA- and PVP/VA-based tablets,
310 respectively, were seen as compared to the theoretical model (Figure 1). Despite the
311 relatively small dimensional variations, the difference is crucial in case of dosage forms
312 printing. Even small deviations might cause an incorrect dose of the API within the
313 printed tablet. The temperature difference and heating/cooling cycling during the printing
314 process are the main reasons for layer warping and shrinkage effects [21]. This issue can
315 be compensated by adding offset values selected according to the formulation content and
316 API concentration. These may be related to additional adhesion of the powder to the
317 printed structures (due to over-sintering) and/or to tablet shrinkage during the cooling
318 process [21].

319 The recorded friability was found to be < 1 wt% for all but two and four batches of
320 the PVA- and PVP/VA-based dosage forms, respectively. Thus, the majority of the
321 printed tablets were in compliance with the specifications (< 1.0 wt% friability) given by
322 the European Pharmacopoeia 2.9.7 – Friability of Uncoated Tablets (Ed. 10.0) [31]. The
323 PVA-based placebo tablets containing 0.5 wt% AC and printed at 2 and 2.5 LPR were
324 observed to be insufficiently sintered, resulting in a higher tablet weight loss of 1.31 and
325 1.11 wt%, respectively (Table S4). Similarly, all PVP/VA-based naproxen-loaded

326 batches and the placebo tablets containing 1 wt% AC printed at an LPR of 3 were
327 observed to be well-sintered, resulting in a tablet weight loss < 0.85 wt% (Table S5). A
328 decreasing trend in friability was also observed with increasing LPR, which was expected
329 due to the densification of the structures arising from a higher degree of sintering (i.e. due
330 to the partial melting and subsequent re-solidification of the polymers/API).

331 X-ray microtomography (μ CT) images of the placebo and naproxen-loaded PVA-based
332 tablets (Figure 7), show a clear decrease in observable porosity with increasing LPR. The
333 following computation showed that the volume fraction of pores is 21.4% and 13.2% in
334 case of PVA-1-2 and PVA-1-3, respectively. This confirms that the previous observations
335 regarding the increase in tablet weight may indeed be partially explained by a structural
336 densification. However, the pore volume fraction in case of the API-loaded structure
337 (PVA-N-1-3) reached 31.9%. An increase in the porosity is likely caused by the denser
338 API-polymer fusion during the sintering process and its following solidification and
339 shrinkage.

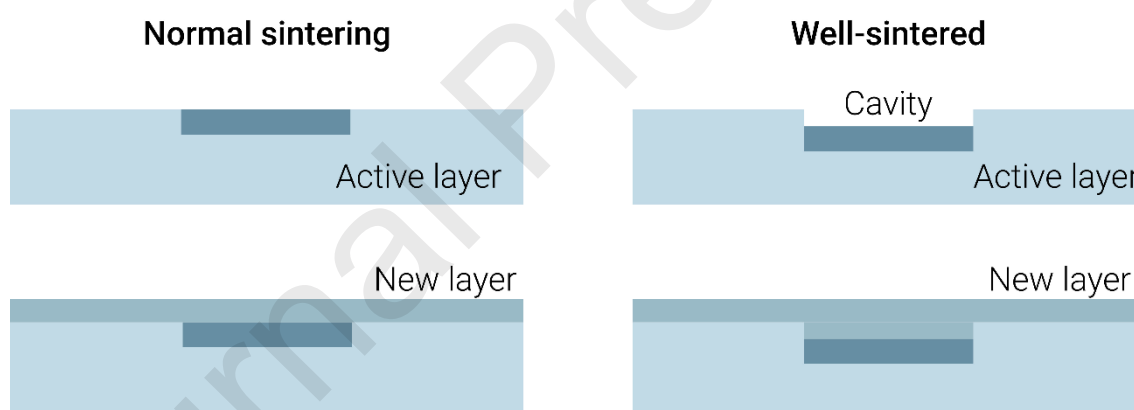


340

341 **Figure 7.** μ CT images of placebo and naproxen-loaded PVA-based tablets containing 1
342 wt% AC and printed at LPRs of 2 and 3.

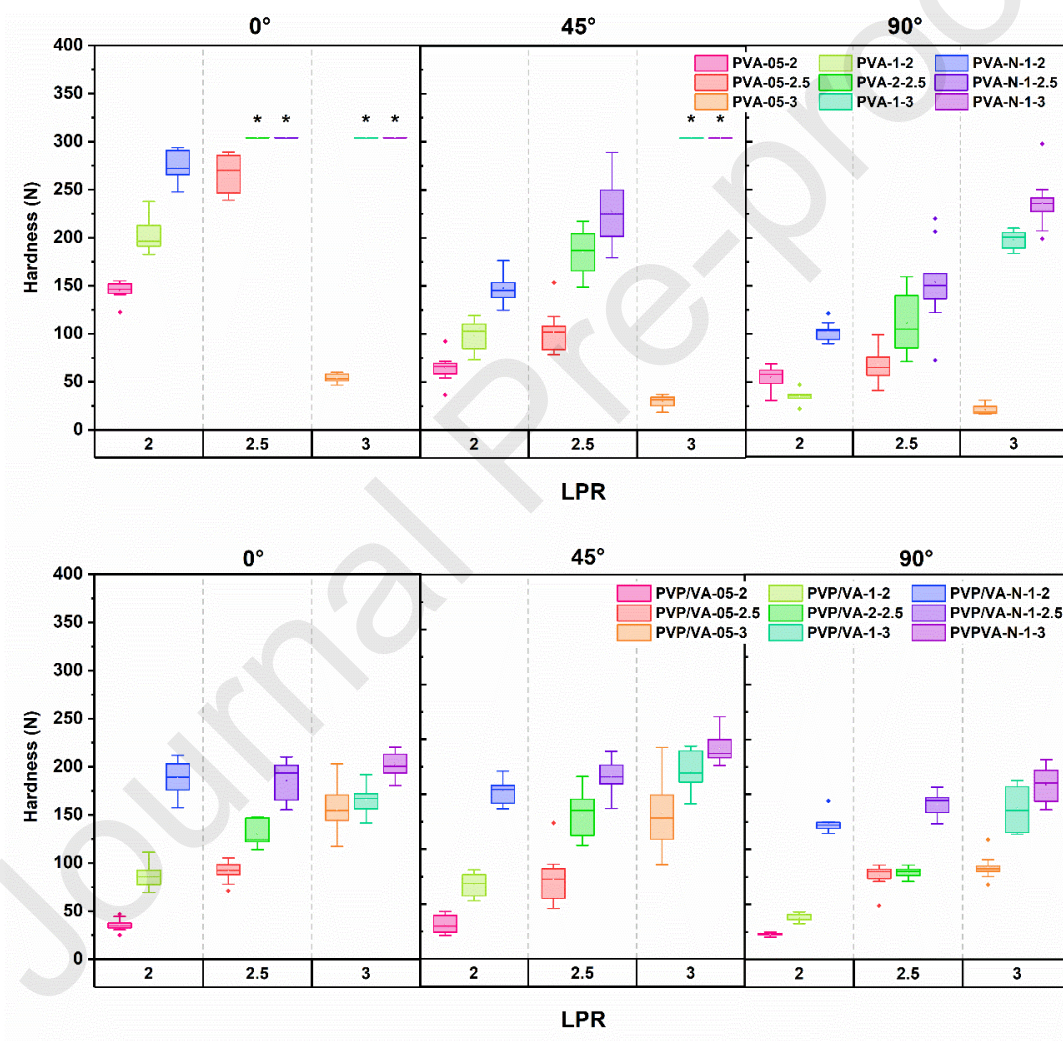
343 Due to the higher LPR and hence the higher thermal energy absorbed by the powder bed,
344 actual melting of the polymer occurs. The molten polymer fills the voids between the

345 particles and dissolves the API in its matrix, resulting in the formation of cavities (Figure
 346 8). These cavities follow the shape of the newly printed layer and are filled with additional
 347 powder after the fresh layer has been applied. The intralayer porosity can be seen to
 348 become less homogenous as the LPR increases. The formation of apparently isolated
 349 cavities within the layers, which may arise from incomplete sintering of adjacent lines, is
 350 observed. The addition of 10 wt% naproxen to the formulation further amplifies these
 351 macroscopic features characterized by a different particle shape (Figure S1) and possibly
 352 indicates that the API and/or colorant may be present as smaller aggregates (Table S3).
 353 Thus, it may lead to a local variation in degree of sintering within the layer. Changes in
 354 the degree of porosity lead to changes in the dissolution behavior due to the close/open
 355 access to the dissolution medium [33].



356
 357 **Figure 8.** Cavity formation and following densification process in case of well-sintering.
 358 The hardness of the PVP/VA-based placebo tablets were further evaluated as a function
 359 of printing angle (Figure 9). A significant difference ($P < 0.05$) in tablet hardness was
 360 observed between the tablets printed at 0° , 45° , and 90° to the print plate. Such anisotropic
 361 response to mechanical stress has previously been reported for other SLS printed
 362 structures and mainly arises from differences in particle sintering within and between
 363 each printed layer (i.e., variations in layer adhesion in the xy -plane as well as along the z -

364 axis) [45]. A decrease in hardness could be observed with increasing print angle and was
 365 found to be due to the applied mechanical stress aligning with the printed layers. Thus,
 366 showing that the inter-layer sintering along the z -axis was weaker as compared to the
 367 sintering in the xy -plane. Further, the hardness of the tablets was also found to be
 368 dependent on the carbon concentration and LPR, which was expected due to a higher
 369 degree of sintering.



370

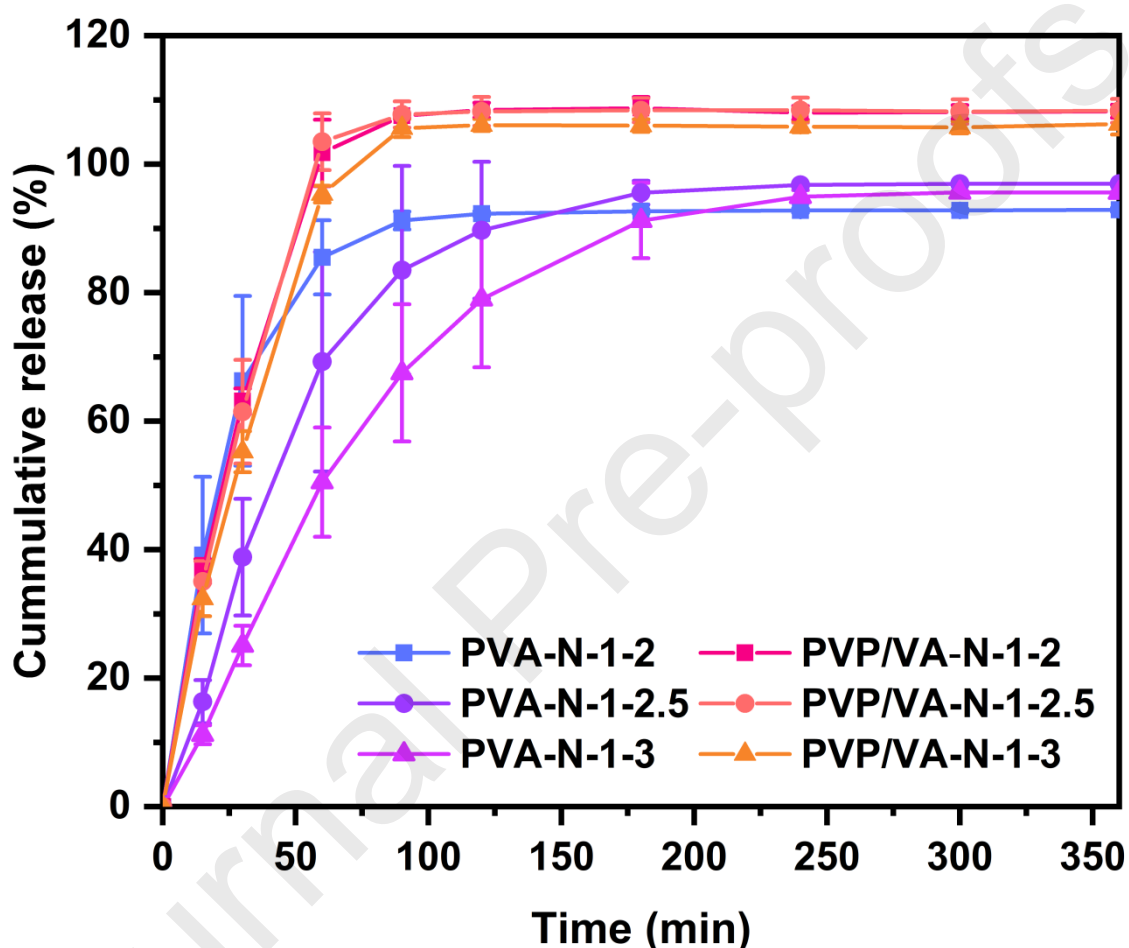
371 **Figure 9.** Boxplots showing the correlation between tablet hardness and printing angle
 372 for (a) the PVA-based and (b) PVP/VA-based tablets ($n = 12$). Tablets exceeding 310 N
 373 in hardness are highlighted in the figure with asterisks.

374

375 3.3 Drug release

376 Drug release profiles of the naproxen-loaded tablets in pH 6.8 phosphate buffer (Figure
377 10) show that 90% of the drug content was released within 180 min and 60 min for the
378 PVA- and PVP/VA-based tablets, respectively. Even though dissolution appears to be
379 complete after 120 min in case of PVP/VA-based formulations, deviations from the
380 expected release of 100 % were observed. Potential reasons might be inhomogeneities in
381 the powder blend or absorption of drug to the polymers. As the focus of this study was a
382 comparison of polymers in SLS, we did not investigate this issue further. Tablets sintered
383 using the lowest and highest LPRs (i.e. PVA-N-1-2, PVA-N-1-3 and PVP/VA-N-1-2,
384 PVP/VA-N-1-3) were observed to have the fastest and slowest drug release rates,
385 respectively. Particularly in the case of the PVA-based tablets, where a 90% drug release
386 was reached within 90 and 180 min, respectively. However, a significant swelling of
387 PVA-based dosage forms was observed within the first two hours because of the low
388 solubility of the polymer in the high pH environment. This caused the variation in
389 cumulative release within triplicates. This feature of PVA is well-known and was
390 described previously in case of FDM printed capsules for drug delivery [46]. Differences
391 in release rate between the batches were however less apparent in the PVP/VA-based
392 tablets, indicating that PVP/VA may be less responsive to changes in LPR as compared
393 to PVA. The dissolution behavior of the printed tablets was found to correspond well with
394 the results obtained from the μ CT images regarding the densification of the structures
395 (Figure 7) with increasing carbon concentration and LPR. This shows that the release rate
396 of the API can be tailored by changing the energy input of the laser during the printing
397 process by producing structures of varying densities. According to recent studies [33, 34],
398 the dissolution profile can vary depending on the sintering degree. In case of a higher

399 amount of heat energy transferred upon the printing layer, the layers interact stronger and
 400 voids between powder particles are filled by viscous polymer after passing the T_g -point.
 401 In case of high scanning speed and using highly-soluble polymers such as Kollidon 90%
 402 of the API can be released within 5 minutes and disintegration can occur within 15 s [47].



403

404 **Figure 10.** Drug release profiles of PVA- and PVP/VA-based naproxen-loaded tablets (n
 405 = 3) in pH 6.8 phosphate buffer.

406 The average drug loading of the naproxen-loaded tablets (Table 2) were shown to be
 407 slightly lower than the theoretical loading of 10 wt%. Both PVA, PVP/VA, and naproxen
 408 were shown to be thermally stable in the temperature range used to print the dosage forms
 409 (Figure S5) and no evidence of drug degradation was observed according to HPLC
 410 analysis. Thus, the lower drug loading may be related to a loss of the API during the

411 powder preparation process. Deviations in the drug content within each batch was found
 412 to be < 0.35 wt% and, thus, the mixing of the powder formulations during the preparation
 413 process were assumed to be sufficient.

414 **Table 2.** Average drug loading of naproxen-loaded tablets (n = 5).

Formulation	Drug loading (wt%)	Drug loading (mg per tablet)	Tablet weight (mg)
PVA-N-1-2	9.42 ± 0.12	31.11 ± 0.71	330.29 ± 3.50
PVA-N-1-2.5	9.04 ± 0.22	32.68 ± 0.57	361.41 ± 3.43
PVA-N-1-3	9.08 ± 0.06	36.14 ± 0.27	398.22 ± 2.48
PVP/VA-N-1-2	9.0 ± 0.23	34.18 ± 0.67	379.88 ± 2.47
PVP/VA-N-1-2.5	8.8 ± 0.14	32.83 ± 1.52	375.22 ± 23.31
PVP/VA-N-1-3	8.7 ± 0.34	34.26 ± 1.53	393.32 ± 5.61

415 4. Conclusions

416 PVA- and PVP/VA-based placebo as well as naproxen-loaded tablets were successfully
 417 printed using a selective laser sintering 3D printing technique. The weight and hardness
 418 of the printed tablets could be tailored by either changing the laser energy input or the
 419 colorant concentration in the formulations. *In-situ* amorphization of the API at 10 wt%
 420 loading was achieved during the printing process for both polymers without any

421 observable degradation of the drug. Further, the release rate of the API from the printed
422 structures could be tailored by changing the laser energy input or the colorant
423 concentration in the formulations, producing structures of varying porosities. PVA-based
424 placebo tablets showed better friability results compared to PVP/VA-based, whereas
425 drug-loaded batches have mass losses of less than 1 wt% for both polymers. However,
426 PVP/VA-based naproxen-loaded tablets have poor mass uniformity which is caused by
427 the higher glass transition point and, consequently, worse polymer/drug interaction during
428 sintering process at the selected printing temperature of 85 °C. This study demonstrates
429 that SLS 3D printing may be a promising technique for manufacturing large batches of
430 solid dosage forms from polymers with different physical properties. Nevertheless, many
431 parameters affect the final printed structures, among others, temperature, LPR,
432 concentration of the colorant and API. The effect of each parameter can be estimated
433 empirically and/or in combination with Quality by Design methods. This study shows, as
434 mentioned above, that the LPR or laser sintering speed has the largest impact on the print
435 outcome. Thus, producing tablets with tailorable properties for personalized medicines.
436 Future studies exploring the drug-polymer interactions and drug release behavior of the
437 API-loaded tablets will be crucial in further evaluating this technique.

438 **Acknowledgements**

439 Thanks are due to Kokott Marcel for assistance with the experiments and performing X-
440 ray micro-computed tomography. Many thanks are due to Mark Carroll for performing
441 analysis and volume fraction of pores computation. Funding by Merck KGaA is
442 gratefully acknowledged. Funding by the Erling-Persson Family Foundation (2017) is
443 gratefully acknowledged. This work is conducted within the Additive Manufacturing for
444 the Life Sciences Competence Center (AM4Life). The authors gratefully acknowledge

445 financial support from Sweden's Innovation Agency VINNOVA (Grant no: 2019-
446 00029)

447

448 References

- 449 [1] R. Kader, G. Liminga, G. Ljungman, M. Paulsson, *Manipulations of oral medications in*
450 *paediatric neurology and oncology care at a Swedish university hospital: Health professionals'*
451 *attitudes and sources of information*, *Pharmaceutics*, 13, (2021), pp. 1676,
452 <https://doi.org/10.3390/pharmaceutics13101676>
- 453 [2] A.C. van der Vossen, L. Al-Hassany, S. Buljac, J.-D. Brugma, A.G. Vulto, L.M. Hanff,
454 *Manipulation of oral medication for children by parents and nurses occurs frequently and is*
455 *often not supported by instructions*, *Acta Paediatr*, 108, (2019), pp. 1475-1481,
456 <https://doi.org/10.1111/apa.14718>
- 457 [3] I. El Aita, J. Rahman, J. Breikreutz, J. Quodbach, *3D-Printing with precise layer-wise dose*
458 *adjustments for paediatric use via pressure-assisted microsyringe printing*, *Eur. J. Pharm.*
459 *Biopharm.*, 157, (2020), pp. 59-65, <https://doi.org/10.1016/j.ejpb.2020.09.012>
- 460 [4] S.J. Trenfield, A. Awad, A. Goyanes, S. Gaisford, A.W. Basit, *3D printing pharmaceuticals:*
461 *Drug development to frontline care*, *Trends Pharmacol. Sci.*, 39, (2018), pp. 440-451,
462 <https://doi.org/10.1016/j.tips.2018.02.006>
- 463 [5] N.A. Charoo, S.F. Barakh Ali, E.M. Mohamed, M.A. Kuttolamadom, T. Ozkan, M.A. Khan, Z.
464 Rahman, *Selective laser sintering 3D printing - an overview of the technology and*
465 *pharmaceutical applications*, *Drug Dev. Ind. Pharm.*, 46, (2020), pp. 869-877,
466 <https://doi.org/10.1080/03639045.2020.1764027>
- 467 [6] A.A. Konta, M. Garcia-Pina, D.R. Serrano, *Personalised 3D printed medicines: Which*
468 *techniques and polymers are more successful?*, *Bioeng.*, 4, (2017), pp.,
469 <https://doi.org/10.3390/bioengineering4040079>
- 470 [7] I. Seoane-Viano, S.J. Trenfield, A.W. Basit, A. Goyanes, *Translating 3D printed*
471 *pharmaceuticals: From hype to real-world clinical applications*, *Adv. Drug Deliv. Rev.*, 174,
472 (2021), pp. 553-575, <https://doi.org/10.1016/j.addr.2021.05.003>
- 473 [8] S. Cailleaux, N.M. Sanchez-Ballester, Y.A. Gueche, B. Bataille, I. Soulaïrol, *Fused deposition*
474 *modeling (FDM), the new asset for the production of tailored medicines*, *J. Control Release*,
475 330, (2021), pp. 821-841, <https://doi.org/10.1016/j.jconrel.2020.10.056>
- 476 [9] H.E. Gultekin, S. Tort, F. Acarturk, *An effective technology for the development of*
477 *immediate release solid dosage forms containing low-dose drug: Fused deposition modeling 3D*
478 *printing*, *Pharm. Res.*, 36, (2019), pp. 128, <https://doi.org/10.1007/s11095-019-2655-y>
- 479 [10] G. Kollamaram, D.M. Croker, G.M. Walker, A. Goyanes, A.W. Basit, S. Gaisford, *Low*
480 *temperature fused deposition modeling (FDM) 3D printing of thermolabile drugs*, *Int. J. Pharm.*,
481 545, (2018), pp. 144-152, <https://doi.org/10.1016/j.ijpharm.2018.04.055>
- 482 [11] K. Sen, T. Mehta, S. Sansare, L. Sharifi, A.W.K. Ma, B. Chaudhuri, *Pharmaceutical*
483 *applications of powder-based binder jet 3D printing process - A review*, *Adv. Drug Deliv. Rev.*,
484 177, (2021), pp. 113943, <https://doi.org/10.1016/j.addr.2021.113943>
- 485 [12] S.Y. Chang, S.W. Li, K. Kowsari, A. Shetty, L. Sorrells, K. Sen, K. Nagapudi, B. Chaudhuri,
486 A.W.K. Ma, *Binder-jet 3D printing of indomethacin-laden pharmaceutical dosage forms*, *J.*
487 *Pharm. Sci.*, 109, (2020), pp. 3054-3063, <https://doi.org/10.1016/j.xphs.2020.06.027>

- 488 [13] A.V. Healy, E. Fuenmayor, P. Doran, L.M. Geever, C.L. Higginbotham, J.G. Lyons, *Additive*
489 *manufacturing of personalized pharmaceutical dosage forms via stereolithography*,
490 *Pharmaceutics*, 11, (2019), pp., <https://doi.org/10.3390/pharmaceutics11120645>
- 491 [14] P.R. Martinez, A. Goyanes, A.W. Basit, S. Gaisford, *Influence of geometry on the drug*
492 *release profiles of stereolithographic (SLA) 3D-printed tablets*, *AAPS PharmSciTech*, 19, (2018),
493 pp. 3355-3361, <https://doi.org/10.1208/s12249-018-1075-3>
- 494 [15] J. Wang, A. Goyanes, S. Gaisford, A.W. Basit, *Stereolithographic (SLA) 3D printing of oral*
495 *modified-release dosage forms*, *Int. J. Pharm.*, 503, (2016), pp. 207-212,
496 <https://doi.org/10.1016/j.ijpharm.2016.03.016>
- 497 [16] F. Fina, C.M. Madla, A. Goyanes, J. Zhang, S. Gaisford, A.W. Basit, *Fabricating 3D printed*
498 *orally disintegrating printlets using selective laser sintering*, *Int. J. Pharm.*, 541, (2018), pp. 101-
499 107, <https://doi.org/10.1016/j.ijpharm.2018.02.015>
- 500 [17] Y.A. Gueche, N.M. Sanchez-Ballester, S. Cailleaux, B. Bataille, I. Soulairol, *Selective laser*
501 *sintering (SLS), a new chapter in the production of solid oral forms (SOFs) by 3D printing*,
502 *Pharmaceutics*, 13, (2021), pp., <https://doi.org/10.3390/pharmaceutics13081212>
- 503 [18] F. Fina, A. Goyanes, C.M. Madla, A. Awad, S.J. Trenfield, J.M. Kuek, P. Patel, S. Gaisford,
504 A.W. Basit, *3D printing of drug-loaded gyroid lattices using selective laser sintering*, *Int. J.*
505 *Pharm.*, 547, (2018), pp. 44-52, <https://doi.org/10.1016/j.ijpharm.2018.05.044>
- 506 [19] F. Fina, A. Goyanes, S. Gaisford, A.W. Basit, *Selective laser sintering (SLS) 3D printing of*
507 *medicines*, *Int. J. Pharm.*, 529, (2017), pp. 285-293,
508 <https://doi.org/10.1016/j.ijpharm.2017.06.082>
- 509 [20] Y.A. Gueche, N.M. Sanchez-Ballester, B. Bataille, A. Aubert, L. Leclercq, J.-C. Rossi, I.
510 Soulairol, *Selective laser sintering of solid oral dosage forms with copovidone and paracetamol*
511 *using a CO₂ laser*, *Pharmaceutics*, 13, (2021), pp. 160,
512 <https://doi.org/10.3390/pharmaceutics13020160>
- 513 [21] M. Schmid, *Laser sintering with plastics: Technology, processes, and materials*, 1st ed.,
514 Hanser, Munich, 2018.
- 515 [22] A. Awad, F. Fina, A. Goyanes, S. Gaisford, A.W. Basit, *3D printing: Principles and*
516 *pharmaceutical applications of selective laser sintering*, *Int. J. Pharm.*, 586, (2020), pp. 119594,
517 <https://doi.org/10.1016/j.ijpharm.2020.119594>
- 518 [23] A. Awad, F. Fina, A. Goyanes, S. Gaisford, A.W. Basit, *Advances in powder bed fusion 3D*
519 *printing in drug delivery and healthcare*, *Adv. Drug Deliv. Rev.*, 174, (2021), pp. 406-424,
520 <https://doi.org/10.1016/j.addr.2021.04.025>
- 521 [24] S. Santitewagun, R. Thakkar, J.A. Zeitler, M. Maniruzzaman, *Detecting crystallinity using*
522 *terahertz spectroscopy in 3D printed amorphous solid dispersions*, *Mol. Pharm.*, 19, (2022), pp.
523 2380-2389, <https://doi.org/10.1021/acs.molpharmaceut.2c00163>
- 524 [25] S.J. Trenfield, H.X. Tan, A. Goyanes, D. Wilsdon, M. Rowland, S. Gaisford, A.W. Basit, *Non-*
525 *destructive dose verification of two drugs within 3D printed polyprintlets*, *Int. J. Pharm.*, 577,
526 (2020), pp. 119066, <https://doi.org/10.1016/j.ijpharm.2020.119066>
- 527 [26] M. Madžarević, Đ. Medarević, S. Pavlović, B. Ivković, J. Đuriš, S. Ibrić, *Understanding the*
528 *effect of energy density and formulation factors on the printability and characteristics of SLS*
529 *irbesartan tablets-application of the decision tree model*, *Pharmaceutics*, 13, (2021), pp. 1969,
530 <https://doi.org/10.3390/pharmaceutics13111969>
- 531 [27] S.J. Trenfield, P. Januskaite, A. Goyanes, D. Wilsdon, M. Rowland, S. Gaisford, A.W. Basit,
532 *Prediction of solid-state form of SLS 3D printed medicines using NIR and Raman spectroscopy*,
533 *Pharmaceutics*, 14, (2022), pp. 589, <https://doi.org/10.3390/pharmaceutics14030589>
- 534 [28] R. Thakkar, M.O. Jara, S. Swinnea, A.R. Pillai, M. Maniruzzaman, *Impact of laser speed and*
535 *drug particle size on selective laser sintering 3D printing of amorphous solid dispersions*,
536 *Pharmaceutics*, 13, (2021), pp., <https://doi.org/10.3390/pharmaceutics13081149>

- 537 [29] D.A. Davis, Jr., R. Thakkar, Y. Su, R.O. Williams, 3rd, M. Maniruzzaman, *Selective laser*
538 *sintering 3-dimensional printing as a single step process to prepare amorphous solid dispersion*
539 *dosage forms for improved solubility and dissolution rate*, J. Pharm. Sci., 110, (2021), pp. 1432-
540 1443, <https://doi.org/10.1016/j.xphs.2020.11.012>
- 541 [30] R. Hamed, E.M. Mohamed, Z. Rahman, M.A. Khan, *3D-printing of lopinavir printlets by*
542 *selective laser sintering and quantification of crystalline fraction by XRPD-chemometric models*,
543 Int. J. Pharm., 592, (2021), pp. 120059, <https://doi.org/10.1016/j.ijpharm.2020.120059>
- 544 [31] European Pharmacopoeia 10th ed., 2.9.7. Friability of Uncoated Tablets, Strasbourg, 2020,
545 pp. 336-337
- 546 [32] The United States Pharmacopeia and National Formulary USP 37–NF 32, <711>
547 Dissolution, The United States Pharmacopeial Convention, Inc., Rockville, MD, 2014,
- 548 [33] P. Kulinowski, P. Malczewski, E. Pesta, M. Łaszcz, A. Mendyk, S. Polak, P. Dorożyński,
549 *Selective laser sintering (SLS) technique for pharmaceutical applications—Development of high*
550 *dose controlled release printlets*, Addit. Manuf., 38, (2021), pp.,
551 <https://doi.org/10.1016/j.addma.2020.101761>
- 552 [34] P. Kulinowski, P. Malczewski, M. Łaszcz, E. Baran, B. Milanowski, M. Kuprianowicz, P.
553 Dorożyński, *Development of composite, reinforced, highly drug-loaded pharmaceutical printlets*
554 *manufactured by selective laser sintering-in search of relevant excipients for pharmaceutical*
555 *3D printing*, Materials, 15, (2022), pp. 2142, <https://doi.org/10.3390/ma15062142>
- 556 [35] S. Lekurwale, T. Karanwad, S. Banerjee, *Selective laser sintering (SLS) of 3D printlets using*
557 *a 3D printer comprised of IR/red-diode laser*, Ann. 3D Print. Med., 6, (2022), pp.,
558 <https://doi.org/10.1016/j.stlm.2022.100054>
- 559 [36] R. Thakkar, D.A. Davis, Jr., R.O. Williams, 3rd, M. Maniruzzaman, *Selective laser sintering*
560 *of a photosensitive drug: Impact of processing and formulation parameters on degradation,*
561 *solid state, and quality of 3D-printed dosage forms*, Mol. Pharm., 18, (2021), pp. 3894-3908,
562 <https://doi.org/10.1021/acs.molpharmaceut.1c00557>
- 563 [37] E.M. Mohamed, S.F. Barakh Ali, Z. Rahman, S. Dharani, T. Ozkan, M.A. Kuttolamadom,
564 M.A. Khan, *Formulation optimization of selective laser sintering 3D-printed tablets of*
565 *clindamycin palmitate hydrochloride by response surface methodology*, AAPS PharmSciTech,
566 21, (2020), pp. 232, <https://doi.org/10.1208/s12249-020-01775-0>
- 567 [38] M. Schmid, LS materials: Polymer properties, in: M. Schmid (Ed.) *Laser sintering with*
568 *plastics: Technology, processes, and materials*, Hanser, Munich, 2018, pp. 65-99.
- 569 [39] C.W. Bunn, *Crystal structure of polyvinyl alcohol*, Nature, 161, (1948), pp. 929–930,
570 <https://doi.org/10.1038/161929a0>
- 571 [40] S. Dedroog, T. Pas, B. Vergauwen, C. Huygens, G. Van den Mooter, *Solid-state analysis of*
572 *amorphous solid dispersions: Why DSC and XRPD may not be regarded as stand-alone*
573 *techniques*, J. Pharm. Biomed. Anal., 178, (2020), pp. 112937,
574 <https://doi.org/10.1016/j.jpba.2019.112937>
- 575 [41] E. Bordos, M.T. Islam, A.J. Florence, G.W. Halbert, J. Robertson, *Use of terahertz-raman*
576 *spectroscopy to determine solubility of the crystalline active pharmaceutical ingredient in*
577 *polymeric matrices during hot melt extrusion*, Mol. Pharmaceutics, 16, (2019), pp. 4361–4371,
578 <https://doi.org/10.1021/acs.molpharmaceut.9b00703>
- 579 [42] S. Qi, A. Gryczke, P. Belton, D.Q.M. Craig, *Characterisation of solid dispersions of*
580 *paracetamol and EUDRAGIT® prepared by hot-melt extrusion using thermal, microthermal and*
581 *spectroscopic analysis*, Int. J. Pharm., 354, (2008), pp. 158-167,
582 <https://doi.org/10.1016/j.ijpharm.2007.11.048>
- 583 [43] C. Yan, Y. Shi, L. Hao, *Investigation into the differences in the selective laser sintering*
584 *between amorphous and semi-crystalline polymers*, Int. Polym. Process., 26, (2011), pp. 416-
585 423, <https://doi.org/10.3139/217.2452>

- 586 [44] C.A. Chatham, T.E. Long, C.B. Williams, *A review of the process physics and material*
587 *screening methods for polymer powder bed fusion additive manufacturing*, Progress in Polymer
588 Science, 93, (2019), pp. 68-95, <https://doi.org/10.1016/j.progpolymsci.2019.03.003>
589 [45] W. Cooke, R.A. Tomlinson, R. Burguete, D. Johns, G. Vanard, *Anisotropy, homogeneity and*
590 *ageing in an SLS polymer*, Rapid Prototyp. J., 17, (2011), pp. 269-279,
591 <https://doi.org/10.1108/13552541111138397>
592 [46] G. Matijašić, M. Gretić, J. Vinčić, A. Poropat, L. Cuculić, T. Rahelić, *Design and 3D printing*
593 *of multi-compartmental PVA capsules for drug delivery*, Journal of Drug Delivery Science and
594 Technology, 52, (2019), pp. 677-686, <https://doi.org/10.1016/j.jddst.2019.05.037>
595 [47] N. Allahham, F. Fina, C. Marcuta, L. Kraschew, W. Mohr, S. Gaisford, A.W. Basit, A.
596 Goyanes, *Selective laser sintering 3D printing of orally disintegrating printlets containing*
597 *ondansetron*, Pharmaceutics, 12, (2020), pp. 110,
598 <https://doi.org/10.3390/pharmaceutics12020110>

599

600 **Evgenii Tikhomirov**: Conceptualization, Methodology, Investigation, Writing - original
601 draft, Visualization. **Michelle Åhlén**: Conceptualization, Methodology, Investigation,
602 Writing - original draft, Visualization. **Nicole Di Gallo**: Methodology, Investigation. **Maria**
603 **Strømme**: Conceptualization, Writing - review & editing, Supervision, Funding
604 acquisition. **Thomas Kipping**: Conceptualization, Writing - review & editing. **Julian**
605 **Quodbach**: Conceptualization, Writing - review & editing, Supervision. **Jonas Lindh**:
606 Conceptualization, Writing - review & editing, Supervision, Funding acquisition.

607

608

609 Declaration of interests

610

611 The authors declare that they have no known competing financial interests or personal
612 relationships that could have appeared to influence the work reported in this paper.

613

614 The authors declare the following financial interests/personal relationships which may be
615 considered as potential competing interests:

616

Jonas Lindh reports financial support was provided by Merck KGaA.

617

618